

Current Hysteresis Control of a Single Phase Integrated Battery Charger With Active Power Decoupling

An internship report submitted
in partial fulfillment for the award of the degree of

Bachelor of Technology

in

**Electronics and Communication Engineering
(with specialization in Avionics)**

by

Chunduri Sai Abhishek



**Department of Avionics
Indian Institute of Space Science and Technology
Thiruvananthapuram, India**

October 2021

Certificate

This is to certify that the internship report titled ***Current Hysteresis Control of a Single Phase Integrated Battery Charger With Active Power Decoupling*** submitted by **Chunduri Sai Abhishek**, to the Indian Institute of Space Science and Technology, Thiruvananthapuram, in partial fulfillment for the award of the degree **Bachelor of Technology in Electronics and Communication Engineering (with specialization in Avionics)**, is a bonafide record of the original work carried out by him under our supervision. The contents of this report, in full or in parts, have not been submitted to any other Institute or University for the award of any degree or diploma.

Dr. R. Sudharshan Kaarthik
Associate Professor
Department of Avionics

Dr. Deepak Mishra
Associate Professor & Head
Department of Avionics

Place: Thiruvananthapuram
Date: October 2021

Declaration

I declare that this internship report titled ***Current Hysteresis Control of a Single Phase Integrated Battery Charger With Active Power Decoupling*** submitted in partial fulfillment for the award of the degree **Bachelor of Technology in Electronics and Communication Engineering (with specialization in Avionics)** is a record of original work carried out by me under the supervision of **Dr. R. Sudharshan Kaarthik**, and has not formed the basis for the award of any degree, diploma, associateship, fellowship, or other titles in this or any other Institution or University of higher learning. In keeping with the ethical practice in reporting scientific information, due acknowledgments have been made wherever the findings of others have been cited.

Place: Thiruvananthapuram

Chunduri Sai Abhishek

Date: October 2021

(SC18B114)

Acknowledgements

I would like to express my gratitude to my supervisor and mentor, Dr. R. Sudharshan Kaarthik, Associate Professor, Department of Avionics, IIST, for giving me this opportunity to work on this topic as my internship. I am very grateful for the tremendous support and guidance that he has provided me at every stage of my work, making my internship very interesting. I am also thankful to him for patiently clearing my doubts and constantly staying focused and motivated.

I would like to thank Dr. Rajeevan P.P., Associate Professor, Department of Avionics, IIST, for sharing his knowledge and skill in the field of power electronics and for providing me with a strong foundation in AC drives and power converters design.

I would also like to thank Dr. Priyadarshnam, Associate Professor, Department of Avionics, IIST, who has always encouraged me to keep my mind open to explore new ideas and was always patient to listen to all my thoughts and ideas.

I thank my M.Tech senior, Mohit Kumar, for clearing my doubts and all the discussions that helped me develop my understanding of the topic. I would like to thank him for his extensive help in learning and implementing the project by assisting me while performing the simulations.

I sincerely thank my parents and my brother for their constant support. Finally, I would like to thank my seniors and friends, KVLN Mallikarjun, Harshit Reddy Vangala, Anant Kumar, Akshaj Jangiti, Praneeth Varma, Meghana Imandi, Aman Naveen, and Anantha Datta Dhruva, for their suggestions, companionship, and for making interactions in IIST enjoyable.

Chunduri Sai Abhishek

Abstract

In today's world, electric vehicles are starting to get more prominence in the automobile sector. Electric Vehicles (EVs) have a smaller carbon footprint and hence a lesser impact on climate. The number of EVs currently in use is lesser when compared to the number of Internal Combustion Engine (ICE) based vehicles. Typically, there are two types of chargers for EVs: off-board chargers and onboard chargers. With off-board chargers, the vehicle needs to be connected to an external charging circuitry. One setback is the non-availability of a charging network. Onboard chargers have the charger circuit as a part of the EV. Integrated chargers are onboard chargers that will use a single circuit to charge the battery and drive the motor. This will reduce the charger's size, weight, and cost and reduce the EV's charging time.

In this report, a novel single-phase integrated battery charger is discussed. Using a single-phase-based system for charging decreases the dependence on charging stations, as the EV can be charged by connecting to any single-phase grid available in households or industries. Single-phase grid-connected systems often suffer from second harmonic ripple power on the DC link. With the help of an active decoupling technique, the excess energy can be stored in one motor windings. Hence, the second harmonic oscillation of power on the DC side can be eliminated. For the control of current in the decoupling winding, a hysteresis controller is implemented in this report. The hysteresis controller is easy to implement, provides inherent short circuit protection, and ensures that the decoupling current is within the specified limits. The simulation results for the system are also presented in the report.

Contents

List of Figures	xi
List of Tables	xiii
Nomenclature	xv
1 Introduction	1
1.1 Electric Vehicles	1
1.1.1 Classification of Electric Vehicles	1
1.2 Charging Infrastructures Available	2
1.3 Power Train Configuration Used in EVs	4
1.4 Need for Power Factor Correction	5
1.4.1 Unity Power Factor Requirement	5
1.5 Outline of the Report	7
2 Integrated Battery Chargers	8
2.1 Need of Integrated Battery Chargers	8
2.2 Single Phase Front End Converter	10
2.2.1 Design of Parameters in Single Phase FEC	13
2.2.2 Design of Inductor (L_s)	13
2.2.3 Design of DC Link Capacitor (C)	14
2.3 Controller Design Strategy	14
2.3.1 Inner Current Loop	15
2.3.2 Outer Voltage Loop	16
3 Integrated Battery Charger Circuit Design	18
3.1 IBC Circuit and Modes of Operation	19
3.2 Power Decoupling	21

3.2.1	Active Power Decoupling	21
3.2.2	Power Decoupling Analysis	22
3.2.3	Different Modes of the Operation of Power Decoupling	24
3.3	Use of Hysteresis Controller for Decoupling Current	26
4	Motor Model and Simulation Results	30
4.1	Performance of the IBC	30
4.1.1	Power Rating of IBC	33
4.2	Simulation Results	34
4.2.1	Simulation Parameters	34
4.2.2	Steady State Behaviour of FEC	34
4.2.3	Transient Behaviour of FEC	35
4.2.4	Simulation Results of IBC topology with Hysteresis Controller	38
5	Conclusions and Future Works	40
Bibliography		41

List of Figures

1.1	Types of Charging Infrastructures	3
1.2	Three Phase Inverter circuit used in Electric Vehicles.	4
2.1	Single Phase Front End Converter Circuit.	11
2.2	Single Phase FEC Equivalent Model.	11
2.3	Phasor Diagram for : (a) UPF operation (AC-DC) (b) For reverse power flow at UPF (DC-AC).	13
2.4	Inner current loop of FEC.	16
2.5	Outer Voltage loop of FEC.	16
3.1	Power Flow in EV in driving and charging modes.	18
3.2	Integrated Battery Charger Circuit.	19
3.3	IBC Circuit in Charging Mode.	20
3.4	Different modes of the operation of power decoupling.	25
3.5	Switching Pulse Generation for C Leg Motor Winding via Hysteresis Controller.	26
3.6	Conventional Control scheme for IBC topology with decoupling.	28
3.7	Control scheme for IBC topology using Hysteresis controller.	29
4.1	Steady state waveforms for 1- ϕ FEC without decoupling : (a) Grid Voltage V_g (V), (b) Grid Current I_g (A), (c) DC-link Voltage V_{DC} (V),(d) Decoupling Current I_{dec} (A)	35
4.2	Steady state waveforms for 1- ϕ FEC with decoupling : (a) Grid Voltage V_g (V), (b) Grid Current I_g (A), (c) DC-link Voltage V_{DC} (V), (d) Decoupling Current I_{dec} (A)	35
4.3	Steady state current waveforms for 1- ϕ FEC with decoupling : (a) Grid Current I_g (A), (b) Decoupling Current I_{dec} (A), (c) DC-link Current $I_{DC_{link}}$ (A).	36

4.4	Transient waveforms for step load change from half load to full load at time $t = 0.5$ s without decoupling.	36
4.5	Transient waveforms for step load change from half load to full load at time $t = 0.5$ s with decoupling.	37
4.6	Transient waveforms for a uniform increase in reference DC bus voltage (from 380 V to 420 V) for three cycles with decoupling (Ramp-Up Response). .	38
4.7	Transient waveforms for a uniform increase in reference DC bus voltage (from 380 V to 420 V) for three cycles with decoupling (Ramp-Down Re- sponse).	38
4.8	Simulation results with hysteresis control based decoupling engaged (step change in load from half load to full load at $t = 0.5$ s).	39
4.9	(a) Ramp-Up and (b) Ramp-Down Responses of the Hysteresis Control Based Decoupling Loop engaged in IBC Circuit	39

List of Tables

1.1	Classification of EV Charging Technologies [1]	2
3.1	Switch Positions of IBC Circuit in different modes of operation.	20
3.2	Switch Positions for different modes of the operation of power decoupling .	25
4.1	Simulation Parameters for IBC	34

Nomenclature

AC	Alternating Current
BEV	Battery Electric Vehicle
DC	Direct Current
EV	Electric Vehicle
FEC	Front End Converter
IBC	Integrated Battery Charger
ICE	Internal Combustion Engine
IGBT	Insulated Gate Bipolar Transistor
IM	Induction Motor
OBC	On Board Charger
P	Proportional Controller
PCC	Point of Common Coupling
PF	Power Factor
PFC	Power Factor Correction
PHEV	Plug-in Hybrid Electric Vehicle
PI	Proportional-Integral Controller
PWM	Pulse Width Modulation
SP-FEC	Single Phase Front End Converter
SPWM	Sine Triangle Pulse Width Modulation
TF	Transfer Function
UPF	Unity Power Factor

Chapter 1

Introduction

1.1 Electric Vehicles

An electric vehicle (EV) is a vehicle that operates either partially or fully on electric power. EVs operate entirely based on electric power as the fuel, unlike their counterpart ICE (Internal Combustion Engine) vehicles which burn fossil fuels like petrol and diesel to generate power. In today's world, EVs are considered to be a potential alternative to ICE-based vehicles, due to the fact that they are eco-friendly.

1.1.1 Classification of Electric Vehicles

EVs can be classified into two major categories:

- Battery Electric Vehicles (BEV)
- Plug-in Hybrid Electric Vehicles (PHEV)

Battery Electric Vehicles (BEV) are those EVs that rely on rechargeable battery packs for power generation. They have fewer moving parts and thus require lesser maintenance. BEVs can be charged overnight and the batteries can provide enough power for an average journey. The merits of a BEV are that they have low cost and maintenance requirements.

The typical charging time of BEV is around 30 minutes to 12 hours, based on the charging speed and battery pack configuration.

Plug-in Hybrid Electric Vehicles (PHEV) are a hybrid mix of EVs which rely both on rechargeable batteries and petrol/diesel for the generation of power. For short-distance travels, PHEVs are run on batteries and for long journeys, PHEVs can be switched to petrol/diesel for power generation. They have disadvantages of a commercial ICE-based vehicle like maintenance, pollutant emissions, etc.

1.2 Charging Infrastructures Available

Pollutants released from ICE vehicles have a significant impact on the atmosphere and are causing climate change. This is motivating many automobile companies to invest in electric vehicle technology, which has improved features and performance. A significant concern for consumers while purchasing an EV is very little availability of charging infrastructure.

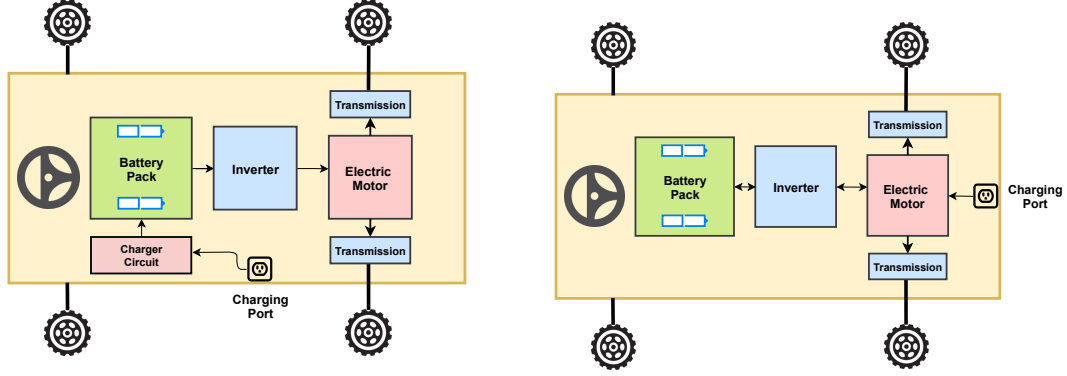
Based on the charger's location, chargers can be categorized into two types:

- On-Board Chargers (AC Charging)
 - Integrated Battery Chargers
- Off-Board Chargers (DC Charging)

Table 1.1: Classification of EV Charging Technologies [1]

S.No	Method of Charging	Category	Power	Time taken for Charging
1	On Board Chargers	Level - 1	1.4 kW	12 - 18 hours
2	Integrated Battery Chargers	Level - 2	3.3 - 6.6 kW	4 - 8 hours
3	Off Board Chargers	Level - 3	20 - 50 kW	15 - 30 minutes

On-board chargers (OBC's) are present inside the electric vehicle and have an extended power outlet for charging the batteries (Fig. 1.1a). They are also referred as Level-One chargers [1]. In AC charging, power conversion is needed between the charging socket



(a) Schematic of a dedicated on-board battery (b) Schematic of an integrated battery charger.

Figure 1.1: Types of Charging Infrastructures

and the battery. So, there will be a charger in the vehicle itself (on-board) and does this power conversion. AC charging is the most flexible, as charging points are ubiquitously available. But, they come with a demerit of adding extra weight, size, and long charging times [2]. AC charging is far less suited to range extension charging, where the distance to travel exceeds the range of the vehicle, as the charging times are simply too long and in this case, the power level of the charger needs to be high for faster charging.

Integrated Battery Chargers (IBC's) are a kind of on-board chargers, but without the requirement of additional circuitry to charge the batteries. The motor and inverter are present in the power train of the vehicle and IBC uses this traction hardware to charge the batteries. The same circuit is switched cleverly in between different configurations for driving and charging modes. Since we are integrating the high-power motor drive into the charging circuit, the power level of the charger increases. Hence, they do not put additional constraints on size, weight, or power level requirements. They are also referred to as Level-Two chargers (Fig. 1.1b). In [3] integrated charging for an electric scooter is discussed.

The last category of chargers are **Off-Board chargers** or also known as Level-Three chargers. They provide DC power directly to the EV i.e., the vehicle is plugged directly into DC that can be fed to the battery. They are located entirely external to the electric

vehicle and all power conditioning (including rectification) is done outside the vehicle [4], [5], and [6]. Hence, they have no constraints on size, weight, or power requirements. DC charging tends to have the highest power ratings and is used for any commercial/public charging station.

1.3 Power Train Configuration Used in EVs

An electric vehicle typically consists of a battery whose power is delivered to the motor. For the power conversion to happen, a DC-AC power converter is required. A three-phase inverter (Fig. 1.2) is generally used for this purpose. The vehicle's batteries supply the mechanical power required for traction in driving mode, and separate charger circuits are used to charge the batteries during the charging mode. During driving mode, batteries supply the power to the motor through the inverter. Different pulse width modulating techniques like sine triangle PWM, Space Vector PWM, etc can be used to switch the inverter and supply the power to the motor.

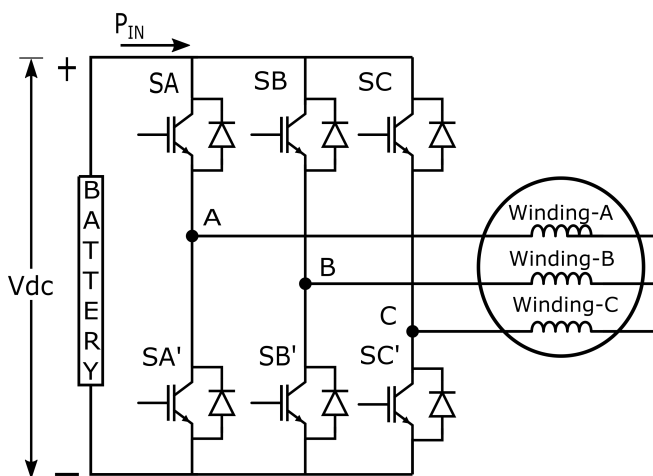


Figure 1.2: Three Phase Inverter circuit used in Electric Vehicles.

1.4 Need for Power Factor Correction

Power Factor (PF) is a measure of how effectively incoming power is used in our electrical system and it is defined as the ratio of real power to apparent power.

$$PF = \frac{Real\ Power(W)}{Apparent\ Power(VA)} = \frac{V_g \cdot I_{g1} \cdot \cos\theta}{V_g \cdot I_g} = \frac{I_{g1} \cdot \cos\theta}{I_g} \quad (1.1)$$

where, V_g is grid voltage, I_g is grid current, I_{g1} is the fundamental component of the grid current and θ is the phase difference between grid voltage (V_g) and fundamental component of the grid current (I_{g1}). [7] The ratio of I_{g1} to I_g is defined as *distortion factor* and $\cos\theta$ is known as the *displacement power factor*. In the absence of any kind of distortion in the grid current, the displacement power factor is conventionally known as the *power factor*.

AC to DC conversion can be done with the diode rectifier, but the problem with diode rectifiers is that they draw non-sinusoidal peaky currents which pollute the grid. Also if the load is non-linear, then non-sinusoidal currents will be drawn from the grid. Since the source impedance value is non-zero, distortion occurs in the grid voltage waveform at the point of common coupling (PCC) where other loads are also connected. This deteriorates the performance of other loads or equipment connected to the PCC or grid.

Power Factor Correction (PFC) is essential for all the non-linear loads connected to the grid as it maximizes the real power drawn from the grid by shaping the input current.

1.4.1 Unity Power Factor Requirement

One of the essential requirements in single-phase grid-connected systems is operating with a unity input power factor. However, because of the Unity Power Factor (UPF) operation, an intrinsic ripple voltage exists on the DC voltage bus in single-phase sinusoidal grid-

connected energy conversion systems, which can be verified as illustrated in (1.2) to (1.3). From (1.4), it can be noted that the magnitude of oscillating power is similar to that of the magnitude of average power during UPF operation.

$$V_{in}(t) = V_g \cos \omega t \quad (1.2)$$

$$I_{in}(t) = I_g \cos \omega t \quad (1.3)$$

$$P_{in}(t) = V_{in}(t) \cdot I_{in}(t) = \frac{V_g \cdot I_g}{2} + \frac{V_g \cdot I_g \cdot \cos(2\omega t)}{2} \quad (1.4)$$

$$P_{in} = P_{avg} + P_{ripple} \quad (1.5)$$

Here $P_{avg} = \frac{V_m \cdot I_m}{2}$, and $P_{ripple} = \frac{V_m \cdot I_m}{2} \cos(2wt)$.

P_{avg} is the power consumed by the load, and P_{ripple} appears across the DC bus. When $P_{in}(t)$ becomes greater than P_{avg} , P_{ripple} flows through DC bus capacitor. While for $P_{in}(t)$ lesser than P_{avg} , ripple power flows back to grid from DC bus capacitor. This causes a ripple of twice frequency to that of fundamental in DC bus voltage. This ripple affects the performance of the DC bus capacitor (causes heating of capacitor), leading to its shorter lifetime. Also, the performance of batteries deteriorates if ripple power flows into them over some time. So it is important to maintain power quality at battery input [8], [9].

In order to mitigate the ripple, several decoupling techniques are used. A few techniques utilize passive components like electrolytic capacitors or an LC resonant branch. Electrolytic capacitors are not suitable for Integrated Battery Charging (IBC) application due to their short lifetime and larger size. An LC resonant branch requires large component's size since resonant frequency must be 100Hz or 50Hz. An alternative to passive component-based decoupling techniques is the active power decoupling technique, which is discussed in the subsequent chapters. The active decoupling of power is also discussed in [10], and [11].

1.5 Outline of the Report

Chapter 1 provides a brief introduction about EVs and their importance in today's context, along with an overview of different types of EVs available in the market. Then, it focuses on the existing charging infrastructures, followed by the merits and demerits of each charging methodology. The later sections of the chapter focus on typical power electronic converters used by EV in its driving mode, followed by the discussion on the requirement of PFC and UPF.

Chapter 2 provides an overview of the Integrated Battery Chargers and their need in today's EV development. Then, a basic single-phase front-end converter (FEC) is discussed. In the later sections of the chapter, the need for an active power decoupling technique is discussed, followed by control loop architectures used in the IBC converter design.

Chapter 3 discussed the IBC converter being designed with its detailed analysis in various modes of EV. This is then followed by the mathematical analysis of the active power decoupling circuit implemented. In the final sections of the chapter, the hysteresis controller and its implementation is discussed.

Chapter 4 is entirely dedicated to the simulation model and the parameters used for simulation. The chapter focuses on the motor model and zero torque production in charging mode. It also discusses the simulation results of the IBC converter for various step and ramp inputs. The results with and without the decoupling circuit are also mentioned, and a note of the improvement achieved is made.

Chapter 5 provides concluding remarks of the work done and presented as a part of this internship, followed by some of the future works that can be done in this project.

Chapter 2

Integrated Battery Chargers

2.1 Need of Integrated Battery Chargers

An onboard charger (OBC) is the most preferred option for EV customers. It provides the flexibility to charge the EV at any location where a single-phase power outlet is available. However, onboard chargers come with the demerit that they would require an extra charger circuit in the EV, which causes an increased cost and weight of the EV. Also, the power rating of these chargers would be low because of their weight and volume constraint. For high power charging requirements, a 3-phase supply with galvanic isolation would be required, increasing the cost and weight of OBC to a considerable extent.

An important observation that is made about EVs is that the vehicle will not be in both charging and driving mode at the same given instant. So, this motivates us to use the traction hardware like motor and inverter, which are already present in the EV's powertrain, for charging the batteries. Doing so will reduce the space and weight of the EV and eliminate the need for an extra charger circuit which was the main demerit of an OBC. This is what is done in Integrated Battery Charging. The charger used in this context is referred to as Integrated Battery Chargers (IBCs). So, to summarize, IBCs are essentially one type of onboard charger, but without the additional requirement of a charger circuit.

The following are the advantages of an IBC over the conventional off-board and on-board chargers :

- **Reduced Cost**

We are utilizing the already existing hardware in the powertrain of EV (like motor, inverter, etc.) for the charging, without using any extra charger. So, the cost of the extra charger or a high-speed charger can be eliminated, and the overall cost of EV comes down.

- **Reduction in Weight**

The batteries of EV can be charged with IBC, and hence we need not carry a separate battery charger (or) on-board charger in the EV. This reduces the vehicle's weight and can contribute to the increased range of the vehicle since one of the factors that determine the range of an EV is its overall weight.

- **Reduced Charging Time**

The power rating of the elements in the powertrain of EV (like motor and inverter) determines the power rating of the IBC. Usually, the powertrain elements have higher power ratings than an onboard charger or separate chargers (except expensive chargers). So this leads to an increased power level of charging and hence a reduced charging time.

- **Charging from a single-phase power outlet**

Usually, for a fast-charging EV, either a 3-phase supply or a separate charging station are required. However, with our single-phase IBC, fast charging of EVs can be achieved even from a 1-phase supply available everywhere. This implies that we can charge the EV faster anywhere with a power supply directly, just with a power cord.

- **Reduction in Footprint**

Due to the absence of on-board chargers or the large bulky filters associated with it, a high power density can be achieved. This is one of the parameters that EV manufacturers aim to achieve.

To develop an IBC, we need to understand a Single-Phase Front End Converter (SP-FEC) basics and how various current and voltage control loops stabilize the grid current and output voltage. The ripple in output voltage is a parameter that will affect the overall efficiency of the EV. Hence, we need to come up with methods to reduce this ripple. The rest of the chapter focuses on these aspects in detail.

2.2 Single Phase Front End Converter

There are various ways in which we can generate a controlled DC output voltage. The standard method to generate this is to use a diode-bridge rectifier, center-tap rectifier, line-commuted rectifier bridge, etc. These diode-based rectifiers have the demerit of being bulky in size, high cost of electronic components used (like the transformers), considerable weight, and a poor dynamic response [12]. Another option available is to use thyristor-based rectifiers. They do not require bulky transformers, and hence the size and weight of the rectifier can be reduced. However, the issue with these rectifiers is that their bidirectional power flow capability is limited. Also, their dynamic response is not that good. They also suffer from high harmonic distortions and poor power factor issues on the grid side. Due to discontinuous current consumption in these rectifiers, pulsed currents are drawn from the grid and cause issues at PCC.

An IGBT-based FEC overcomes all the issues mentioned above: poor dynamic control, harmonic distortions of current, and poor power factor due to high-frequency switching of the semiconductor devices. Hence, in most industrial applications, IGBT-based single-

phase FEC (SP-FEC) is preferred for AC-DC conversion.

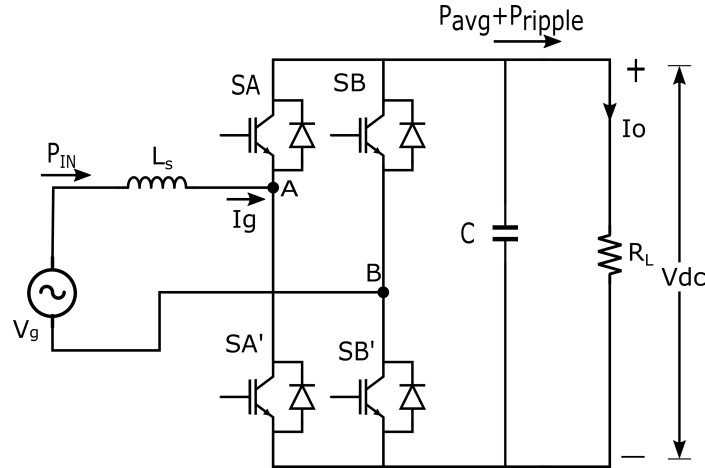


Figure 2.1: Single Phase Front End Converter Circuit.

A typical single-phase FEC circuit is shown in (Fig. 2.1). It consists of a single-phase AC voltage source (V_g), inductor (L_s), full-bridge inverter, DC bus capacitance (C) and a resistive load (R_L). The gating pulses in a conventional SP-FEC circuit are generated using the sine-triangle PWM technique.

The main objectives of the FEC are as follows :

- Regulate the DC Bus Voltage (V_{DC})
- Reduce the Grid side current distortions
- Ensure Bidirectional power flow and UPF operation.

The equivalent model of the SP-FEC mentioned above is as shown in (Fig. 2.2). When

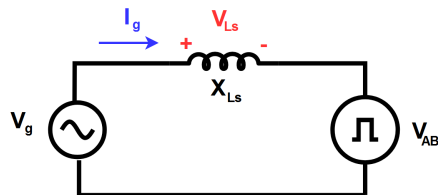


Figure 2.2: Single Phase FEC Equivalent Model.

the grid current and voltage are in phase, the current comes from the grid, and when grid current and voltage are out of phase (180°), current flows back into the grid.

The voltage across converter phase is given by,

$$V_{AB} = V_{AO} - V_{BO} = (S_A - S_B).V_{DC} \quad (2.1)$$

Where S_A, S_B are the switching functions for leg A and B of the converter. While switching modulating signals for both A and B, lags are 180° phase-shifted. Two switches of a particular leg operate in a complementary manner, such that Eq.(2.2) is satisfied. Here, d_A and d_B are the duty ratios of the switching legs A and B, respectively.

$$d_A + d_B = 1 \quad (2.2)$$

From the conventional notion of power systems, it is known that real power flow happens from leading voltage angle to lagging angle and reactive power flows from higher voltage magnitude to lower one. For FEC operation at UPF, both grid voltage and grid current will be in phase, and real power flows from the grid to load (AC to DC side). For lagging pf operation, grid voltage leads V_{AB} and both active and reactive power flows from the grid to load.

In the case of leading pf operation, V_{AB} leads grid voltage, but since it has a lower magnitude than grid voltage, so active power flows from AC to DC side. However, reactive power flows from DC to AC side. In the case of the regenerative mode of operation at UPF V_{AB} leads grid voltage, and only real power flows from DC to AC side.

The phasor diagrams associated with these scenarios are depicted in (Fig. 2.3). Here, δ is defined as the load angle. In either of the cases, we have Unity Power Factor being maintained. Convention followed in the analysis is that current flow from grid to converter is taken as positive, and converter to the grid is taken as negative.

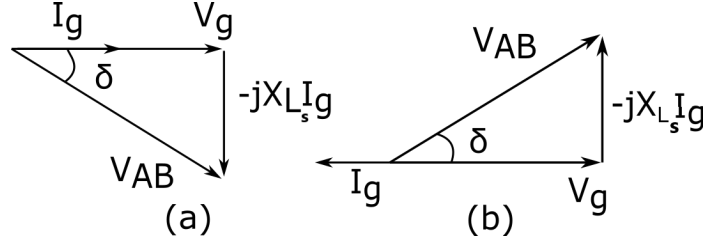


Figure 2.3: Phasor Diagram for : (a) UPF operation (AC-DC) (b) For reverse power flow at UPF (DC-AC).

2.2.1 Design of Parameters in Single Phase FEC

From power balance (assuming no losses),

$$V_{AB}(t) \cdot I_g(t) = V_o I_o \quad (2.3)$$

$$I_o = \frac{|V_{AB} \cdot I_g|}{2V_o} [\cos \delta - \cos(2\omega t - \delta)] \quad (2.4)$$

$$I_o = I_{Load} + I_{cap} \quad (2.5)$$

$$I_{cap} = \frac{|V_{AB} \cdot I_g|}{2V_o} \cos(2\omega t - \delta) \quad (2.6)$$

2.2.2 Design of Inductor (L_s)

There are two ways of designing the inductor value. Equations associated with both approaches are mentioned as follows :

$$|j\omega L_s I_g| \leq \frac{10}{100} V_g \quad (2.7)$$

$$V_g = j\omega L_s I_g + V_{AB} \quad (2.8)$$

$$V_o = \sqrt{V_g^2 + (L_s \omega I_g)^2} \quad (2.9)$$

$$L_s \leq \sqrt{\frac{mV_o^2 - V_{g_{max}}^2}{\omega^2 I_{g_{max}}^2}} \quad (2.10)$$

We can use either Eq.(2.7) or Eq.(2.12), for the design of L_s . We can apply Eq.(2.7) for full load power condition. It is a thumb rule to ensure that only 10% or lesser voltage drop occurs across L_s and the remaining voltage drop appears across the load.

In Eq.(2.12), (m) is the modulation index of the SPWM, V_o is the output DC Bus Voltage, ω is the frequency of grid voltage in (rad/sec). and $I_{g_{max}}$ and $V_{g_{max}}$ are the peak values of grid current and voltage respectively.

2.2.3 Design of DC Link Capacitor (C)

Voltage across the DC Link capacitor can be given as follows (from Eq.2.6):

$$V_c(t) = \frac{i_c t}{C} = \frac{1}{C} \int_0^{\pi/2} I_g \cos(2\omega t) d(2\omega t) = \frac{I_g}{2C\omega} \quad (2.11)$$

$$\frac{I_g}{2C\omega} \leq \Delta V_o \quad (2.12)$$

$$C \geq \frac{mI_g}{8\pi f \Delta V_o} \quad (2.13)$$

Here, in Eq.(2.14) ΔV_o is the ripple allowed in the output DC bus voltage. If this specification is not given, a thumb rule would be to set $\Delta V_o \leq 5\%$ of V_o . If we consider the modulation index of the sine-triangle PWM technique as (m), and f is the frequency of the grid voltage in (Hz), then we can use Eq.(2.15).

2.3 Controller Design Strategy

Two control loops are used in SP-FEC in order to ensure the following :

- Inner Current Loop: This is to ensure the UPF operation, i.e., to always ensure I_g and V_g are in phase.

- Outer Voltage Loop: This ensures that the output DC bus voltage is at the desired value as per specifications [12].

These loops deploy standard P and PI controllers. The inner current loop uses a P controller, and the outer voltage loop uses a PI controller. Their gains have been tuned so that any changes on the load side will reflect the output voltage and current to settle back to its nominal value within five-six fundamental cycles of the switching frequency. For the decoupling circuit, a hysteresis controller is implemented. Hysteresis controller is used to ensure the required decoupling current, and this will be discussed in detail in Chapter 3.

2.3.1 Inner Current Loop

Block diagram for the inner current controller is shown in (Fig.2.4). For designing the controllers, the PWM converter is modeled as a first-order transfer function as given in (2.14). Here, where G is the inverter gain given as per (2.15), and T_d is the maximum time delay of inverter in sine-triangle PWM. T_d is also equal to the time interval of one triangular carrier wave [7].

$$T(s) = \frac{G}{1 + sT_d} \quad (2.14)$$

$$G = \frac{V_{DC}}{\text{carriermax.value}} \quad (2.15)$$

Transfer function (TF) of the inner current loop is given by (2.16). Comparing this with standard second order transfer function in (2.17), we get (2.18). The thumb rule for a good design is to make the system to be critically damped i.e., $\zeta = 0.707$. Substituting $\zeta = 0.707$ and simplifying the equations, we get (2.19). Overall TF of the inner current loop can be approximated as in (2.20).

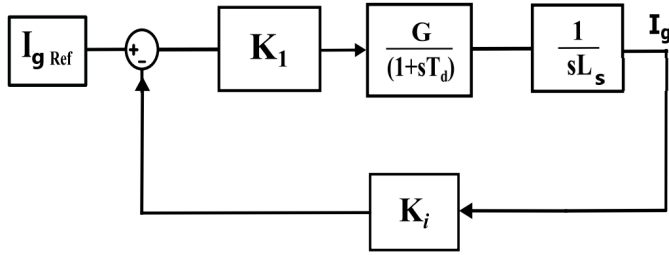


Figure 2.4: Inner current loop of FEC.

$$G(s) = \frac{I_g}{I_{gRef}} = \frac{K_1 G}{s^2 T_d L + s L_s + K_1 K_i G} \quad (2.16)$$

$$G(s) = \frac{\omega_n^2}{s^2 + 2\zeta\omega_n s + \omega_n^2} \quad (2.17)$$

$$2\zeta\omega_n = \frac{1}{T_d}, \omega_n^2 = \frac{K_1 K_i G}{T_d L_s} \quad (2.18)$$

$$K_1 = \frac{L}{T_c K_i G}, T_c = 2T_d \quad (2.19)$$

$$G_c(s) = \frac{\frac{1}{K_i}}{s^2 T_c T_d + s T_c + 1} \quad (2.20)$$

2.3.2 Outer Voltage Loop

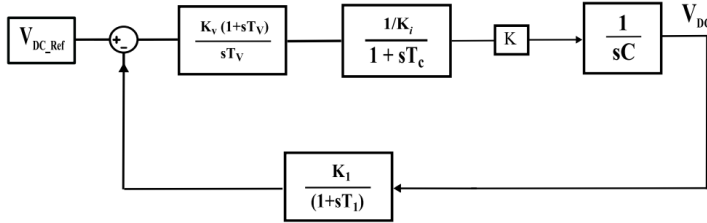


Figure 2.5: Outer Voltage loop of FEC.

The response for the 2nd order system is dominant for only higher frequencies. So, if the reference to this loop is slow, the TF can be equivalent to first-order TF, and the control structure is shown in (Fig.2.5). The overall transfer function of the system $H(s)$ is given

by (2.21).

To design the voltage controller, the symmetric optimization technique or modulus hugging method can be used. Suppose we try to design it using the same method as of current controller. In that case, the voltage controller will make the entire system unstable or marginally stable, which is not desired [7] .

In the symmetric optimization technique, transfer function $H(s)$ is compared to the standard third-order transfer function, and coefficients are equated. The frequency response will have a significant (wide) bandwidth. After equating the coefficients and simplifying the equations, we get (2.22). We can also do the same by using Modulus Hugging Method, doing which gives (2.23).

$$H(s) = \frac{V_{DC}}{V_{DC,Ref}} = \frac{K_v V_g (1 + sT_v)}{2K_i C s^2 T_v V_o (1 + sT_c) + K_2 K_v V_g (1 + sT_v)} \quad (2.21)$$

$$K_v = \frac{CK_i V_o}{K_1 T_c V_g}, T_v = 4T_c \quad (2.22)$$

$$K_v = \frac{K_i V_o C}{3K_1 V_g T_c}, T_v = \frac{4K_i V_o C}{3K_1 K_v V_g} \quad (2.23)$$

Chapter 3

Integrated Battery Charger Circuit Design

In an IBC, the modules present in the powertrain of the EV, like the motor and the inverter are used for the charging of the batteries of EV. (Fig. 3.1) shows the block diagram of an IBC present in EV and the power flow direction in driving and charging modes. The motor windings are used as interface inductors between the grid and inverter module in the charging mode of operation.

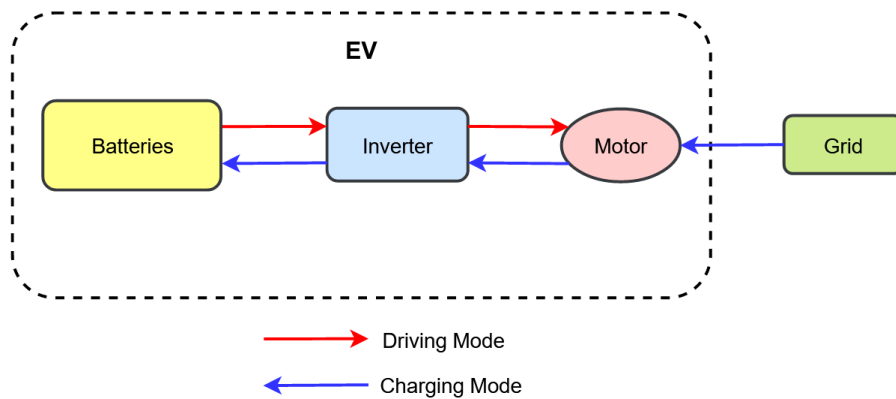


Figure 3.1: Power Flow in EV in driving and charging modes.

The wheels of the EV are modeled as an Induction Motor (IM), and this is shown as the *Motor* block in (Fig. 3.1). In the driving mode, the grid is nowhere connected to

our EV, and batteries supply the required power to the motor (wheels of the EV) via the inverter module (DC to AC). IBC uses the same powertrain of EV in the charging mode, and the grid is connected to the EV. The direction of power flow is now reversed, i.e., the grid supplies the power to the inverter via the motor (which acts as the interface inductor) between them. Then this power is transferred from the inverter module to charge the EV batteries (AC to DC).

3.1 IBC Circuit and Modes of Operation

The IBC converter is shown in (Fig. 3.2). During *motoring (driving of vehicle) mode* of Induction Machine (IM) switch SW is kept open, and SW1, SW2 have their contacts at positions 1 and 1' respectively. Legs A, B, and C act as a three-phase inverter to power drive IM in this mode. The C phase winding is connected between leg B and C of the inverter. It can be seen that there is no extra component required for the configuration other than the contacts, SW, SW1, and SW2. For FEC, an analysis is done in [13].

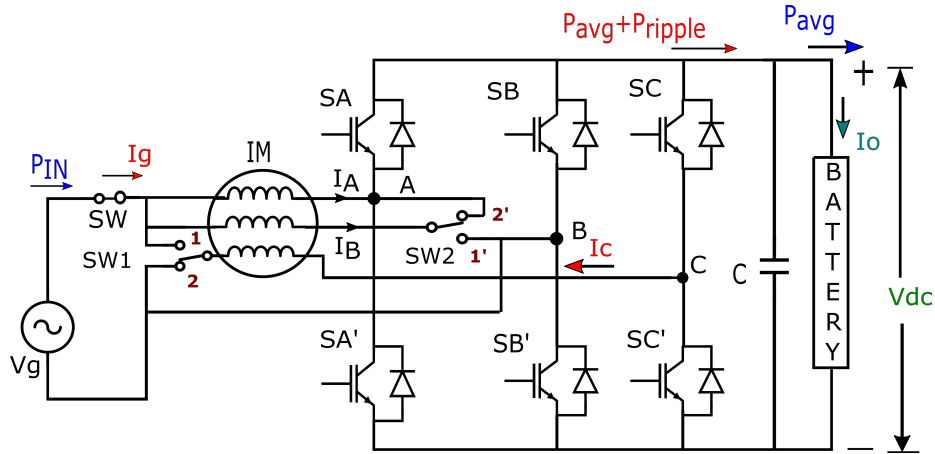


Figure 3.2: Integrated Battery Charger Circuit.

For *charging mode*, IM windings are configured by closing switch SW and changing contacts of SW1, SW2 to position 2 and 2' respectively. This configuration results in A and B phase windings getting parallel and connected between the grid and Leg A of the

S.No	Mode of Operation of EV	SW Position	SW1 Position	SW2 Position
1	Driving Mode (Motoring Mode)	Open	1	1'
2	Charging Mode	Close	2	2'

Table 3.1: Switch Positions of IBC Circuit in different modes of operation.

inverter. In this mode, winding A and B of IM are connected in parallel and serve as interface inductors for a single-phase grid. The C-phase winding is used as a decoupling inductor for the active power decoupling circuit to minimize DC bus voltage ripple.

Two parallel connected A and B phase windings of IM and Leg A and B of inverter act as a grid-connected single-phase AC-DC Front End Converter (FEC). The remaining C phase winding and legs B and C act as a decoupling circuit for ripple minimization in DC bus voltage. The leg B of the inverter is shared between FEC and decoupling circuit for the proposed topology (Fig. 3.3). (Table 3.1) summarizes the switch positions of the IBC circuit in different modes of operation.

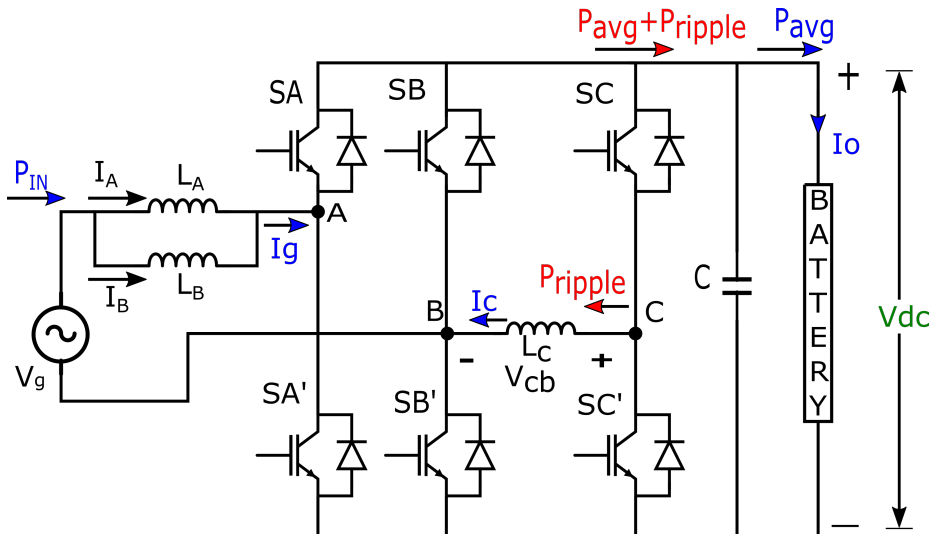


Figure 3.3: IBC Circuit in Charging Mode.

3.2 Power Decoupling

The single-phase IBC design is capable of working with the available single-phase mains supply. As derived in equations (1.2)-(1.5), we observe that the instantaneous ac input power of single-phase systems consists of P_{ripple} in addition to P_{avg} which varies at double the fundamental line frequency (2ω). P_{ripple} in IBCs leads to a significant voltage ripple on the DC bus and thus affects the performance of the battery. While connecting FEC with the grid, current should have minimum harmonic content for avoiding damage coming from non-linear loads[14], [15], and [16]. This can also lead to a temperature rise and hence can bring down the lifetime of the batteries.

The increase in temperature can occur due to second harmonic currents flowing through the battery. The suppression of second-harmonic voltage ripple present on the DC-side of the PFC circuit in an IBC is of utmost importance. There are two methods to eliminate/decrease P_{ripple} : a passive and active method for power decoupling. In the passive method, we use bulky DC capacitors and inductors to filter out the second-harmonic ripple. However, it increases the cost and reduces the power density of the power converter. In the active method, switching devices are used along with energy storage inductors and capacitors.

3.2.1 Active Power Decoupling

The main idea is to divert the ripple power (P_{ripple}) on the DC-link to some energy storage element (either inductor or capacitor).

The leakage inductance of the driving motor is utilized for decoupling purposes and as an input inductor for the IBC circuit. The two legs of the driving inverter are utilized in the charging circuit, and the third leg is utilized in the decoupling circuit. The switching should take place in such a way that when the instantaneous input power (P_{inst}) is greater than

the average input power (P_{avg}), the decoupling inductor should store this excess energy (P_{ripple}). When P_{inst} is less than P_{avg} , the decoupling inductor must release this excess energy (P_{ripple}).

3.2.2 Power Decoupling Analysis

Instantaneous power absorbed by motor windings connected to the grid is given by (3.1). Similar equations and analyses hold for motor winding B as well. Instantaneous power in L_C is as mentioned in (3.3).

$$P_{L_A} = \frac{\omega L_A I_m^2 \sin(2\omega t)}{4} \quad (3.1)$$

Assuming that reference decoupling current through L_C is

$$i_{L_C} = I_{L_C} \sin(\omega t + \alpha) \quad (3.2)$$

$$P_{L_C} = L_C \left(\frac{di_{L_C}}{dt} \right) i_{L_C} = \omega L_C I_{L_C}^2 \sin(2\omega t + 2\alpha) \quad (3.3)$$

From power balance principle,

$$P_{inst} = P_{Load} + 2P_{L_A} + P_{L_C} \quad (3.4)$$

$$P_{Load} + \frac{\omega L_A I_m^2 \sin(2\omega t)}{4} + \frac{\omega L_C I_{L_C}^2 \sin(2\omega t + 2\alpha)}{2} = \frac{V_m \cdot I_m}{2} + \frac{V_m \cdot I_m \cdot \cos(2\omega t)}{2} \quad (3.5)$$

Substituting P_{Load} in (3.4) and defining

$$\phi = \tan^{-1} \left(\frac{\omega L_A I_m}{2V_m} \right)$$

$$I_{L_C} = \sqrt{\frac{(V_m I_m)^2 + \left(\frac{\omega L_C I_m^2}{2} \right)^2}{\omega L_C}} \quad (3.6)$$

$$\alpha = \frac{-\phi}{2} - \frac{\pi}{4} \quad (3.7)$$

For input current at UPF operation,

$$\alpha \approx \frac{\pi}{4}$$

In the decoupling circuit used in our IBC, legs A and B in the FEC circuit and the third winding (i.e., of leg C) of the induction motor is used for decoupling purposes. The third motor winding acts as the decoupling inductor. Leg B is shared mutually between the decoupling and the FEC circuits. The main idea behind an active decoupling circuit is to ensure proper current flow through the decoupling inductance based on Eq.(3.2) - (3.7).

The current through the decoupling inductor is given as in Eq.(3.2). Here, I_{L_C} is the magnitude of decoupling current, ω is the angular frequency of the grid, and α is the phase of decoupling current w.r.t grid voltage. The instantaneous decoupling power is given by Eq.(3.3). The decoupling circuit aims to eliminate the DC output voltage ripple. For this, $P_{ripple}(t) = P_{decoupling}(t)$ should be ensured. As a result, leg-C of the induction motor is modulated to produce a current through the decoupling inductor, whose instantaneous power is the ripple power. The output DC voltage ripple can be decreased in this method. Hence, the predicted waveform of DC output voltage after decoupling is expected to be completely devoid of oscillations.

3.2.3 Different Modes of the Operation of Power Decoupling

There are four modes of operation by which decoupling is happening, as shown in (Fig. 3.4) [7]. The current flowing through the energy storage inductor L_c is constrained by the diode D_B . Here D_B , $D_{B'}$, D_C , $D_{C'}$ are the diodes parallel to S_B , $S_{B'}$, S_C , and $S_{C'}$ respectively.

- **Mode I:**

Switch $S_{B'}$ and $S_{C'}$ are ON while S_C, S_B are OFF. The current freewheels through $D_{C'}, L_c$ and $S_{B'}$. The voltage across inductor (v_{L_c}) is zero so the energy stored does not change in this mode.

- **Mode II:**

Switches S_C, S_B are ON while $S_{B'}$ and S_C are OFF. The current flows through $D_{C'}, L_c, D_B$. The inductor voltage $v_{L_c} = -V_{DC}$. So, the inductor releases the energy and the capacitor is being charged. This mode is called *discharging mode*.

- **Mode III:**

Switches S_B and S_C are ON while $S_{B'}$ and $S_{C'}$ are OFF. The current freewheels through S_C, L_c and D_B . Hence, $v_{L_c} = 0$ and the stored energy does not change.

- **Mode IV:**

Switches S_C and $S_{B'}$ are ON while S_B and $S_{C'}$ are OFF. The current flows through S_C, L_c and $S_{B'}$. The inductor voltage $v_{L_c} = V_{DC}$. So, the inductor stores the energy and the capacitor is being discharged. This mode is called the *charging mode*. All the modes and different switch positions in each mode is summarized in Table-3.2.

So, the average voltage across the inductor over one switching cycle is given by,

$$v_{L_c} = (d'_b - d'_c).V_{DC} \quad (3.8)$$

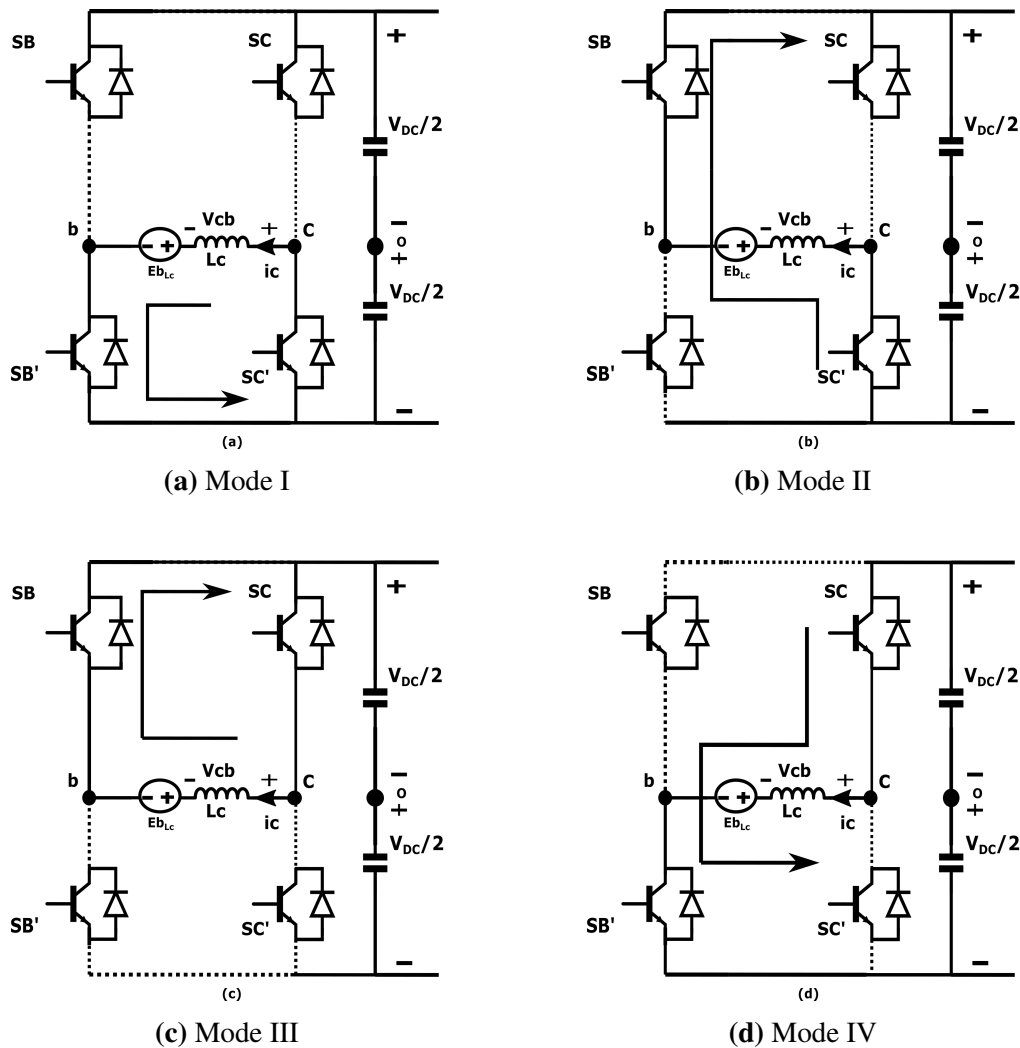


Figure 3.4: Different modes of the operation of power decoupling.

S.No	Mode	SB	SB'	SC	SC'	v_{L_c}
1	Mode I	OFF	ON	OFF	ON	Zero
2	Mode II (Discharging Mode)	ON	OFF	OFF	ON	$-V_{DC}$
3	Mode III	ON	OFF	ON	OFF	Zero
4	Mode IV (Charging Mode)	OFF	ON	ON	OFF	V_{DC}

Table 3.2: Switch Positions for different modes of the operation of power decoupling

where d'_b and d'_c are the duty ratios for bottom switches of leg B and C ($S_{B'}$ and $S_{C'}$), respectively.

3.3 Use of Hysteresis Controller for Decoupling Current

In the IBC circuit design, the FEC works with sine-triangle pulse width modulation (SPWM) scheme. Switching pulses to legs A and B are generated using the standard SPWM approach. Two control loops have been implemented in order to ensure UPF operation and stable output DC voltage. For the decoupling circuit, a *hysteresis controller* is implemented. The job of this hysteresis controller is to generate switching pulses which will ensure the decoupling current (I_{dec}) via inductor L_c is per Eq.(3.2), (3.6), and (3.7).

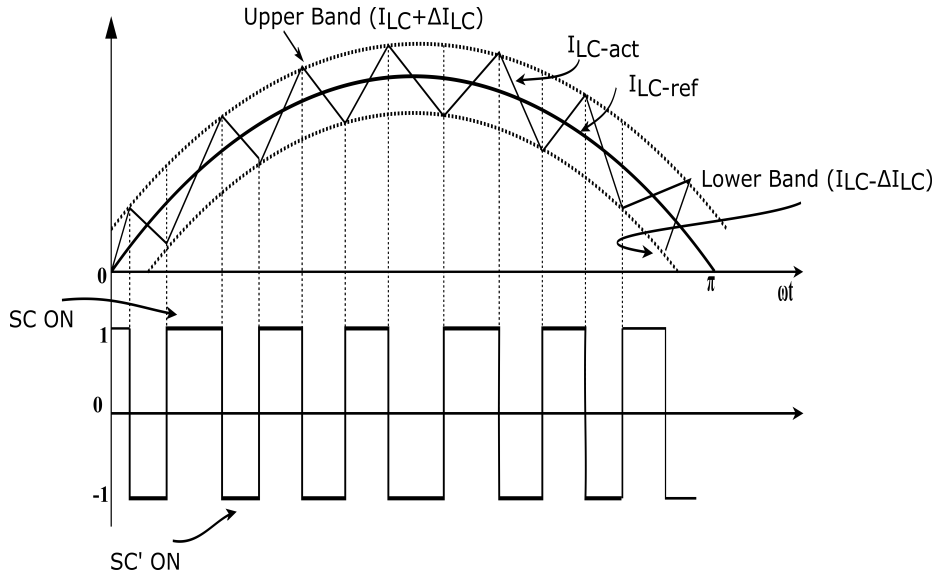


Figure 3.5: Switching Pulse Generation for C Leg Motor Winding via Hysteresis Controller.

Using hysteresis control for the IBC topology provides the following advantages:

- Excellent dynamic performance and ability to control the peak to peak value of current ripple in desired hysteresis band.
- Inherent short circuit protection for grid current.
- Easier controller implementation.

For the simulation case, an error of 500mA from nominal decoupling current is considered. Whenever I_{dec} hits the upper band, the hysteresis controller generates a low switching pulse for the top IGBT device and a high pulse for the bottom IGBT device of the C phase. These pulses are then fed as switching pulses to the top switch in leg-C, and the complementary pulses are given to the bottom switch in leg-C. This switching causes diversion of ripple power in the decoupling inductor, and hence ripple in DC bus voltage is minimized. (Fig. 3.5) shows the switching pulse generation based on the error in I_{dec} .

The conventional control scheme architecture for the IBC topology with decoupling is shown in (Fig.3.6). The overall control scheme architecture of the IBC Charger circuit with hysteresis controller is shown in (Fig.3.7). The simulation model for the discussed control scheme includes inner current loop for controlling grid current at its level and outer voltage loop for regulation of DC- bus voltage [12], a separate current loop is required for controlling decoupling current. The output DC-bus voltage is sensed, compared to a set reference, and the error between the two is fed to the voltage PI controller. The voltage PI gives the magnitude of the reference grid current. A current template identical to grid voltage is multiplied to voltage controller output. This results in a sinusoidal grid current reference,which is now compared with the actual grid current flowing through windings A and B of IM. The P controller in the current loop gives modulating signals for PWM switching of Leg A and B of FEC. For decoupling current loop reference $I_{dec}(t)$ is generated by Eq.(3.2), Eq.(3.6), and Eq.(3.7). The motor C phase winding carries actual $I_{dec}(t)$.

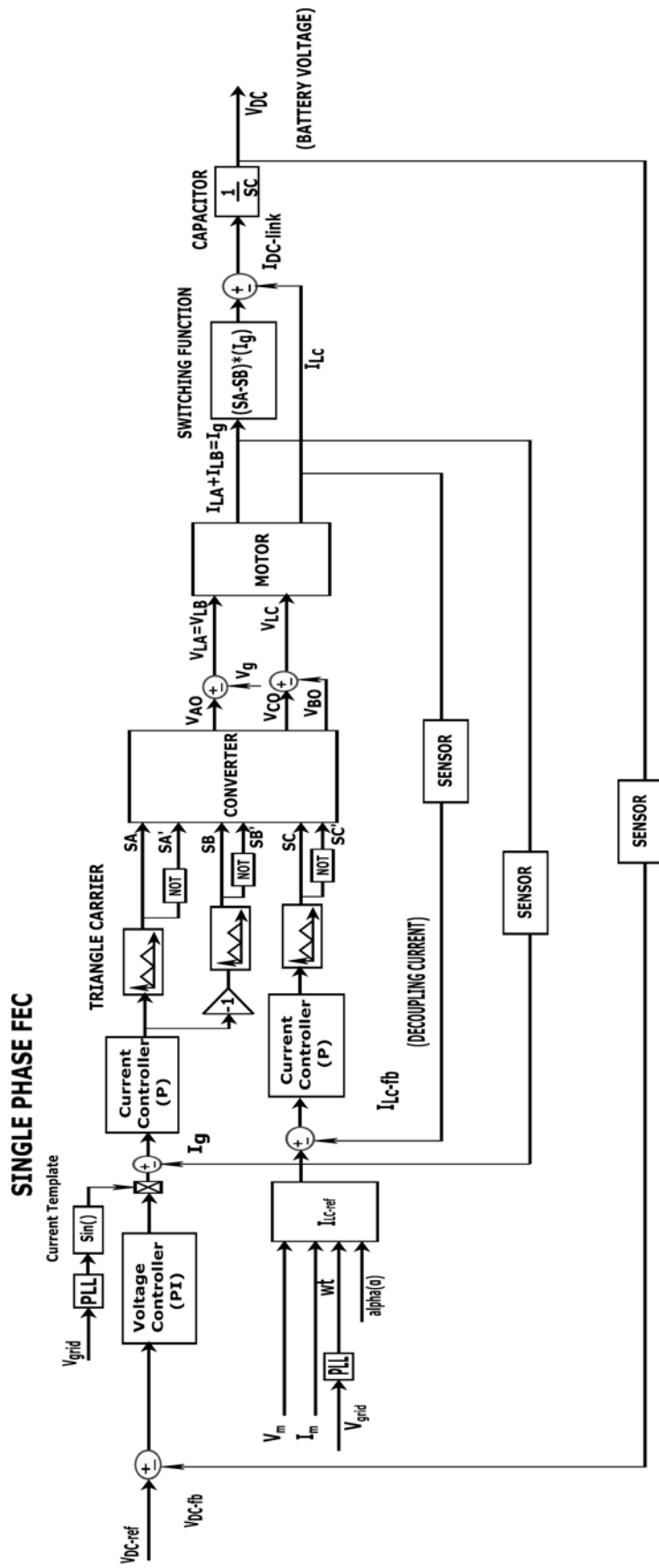


Figure 3.6: Conventional Control scheme for IBC topology with decoupling.

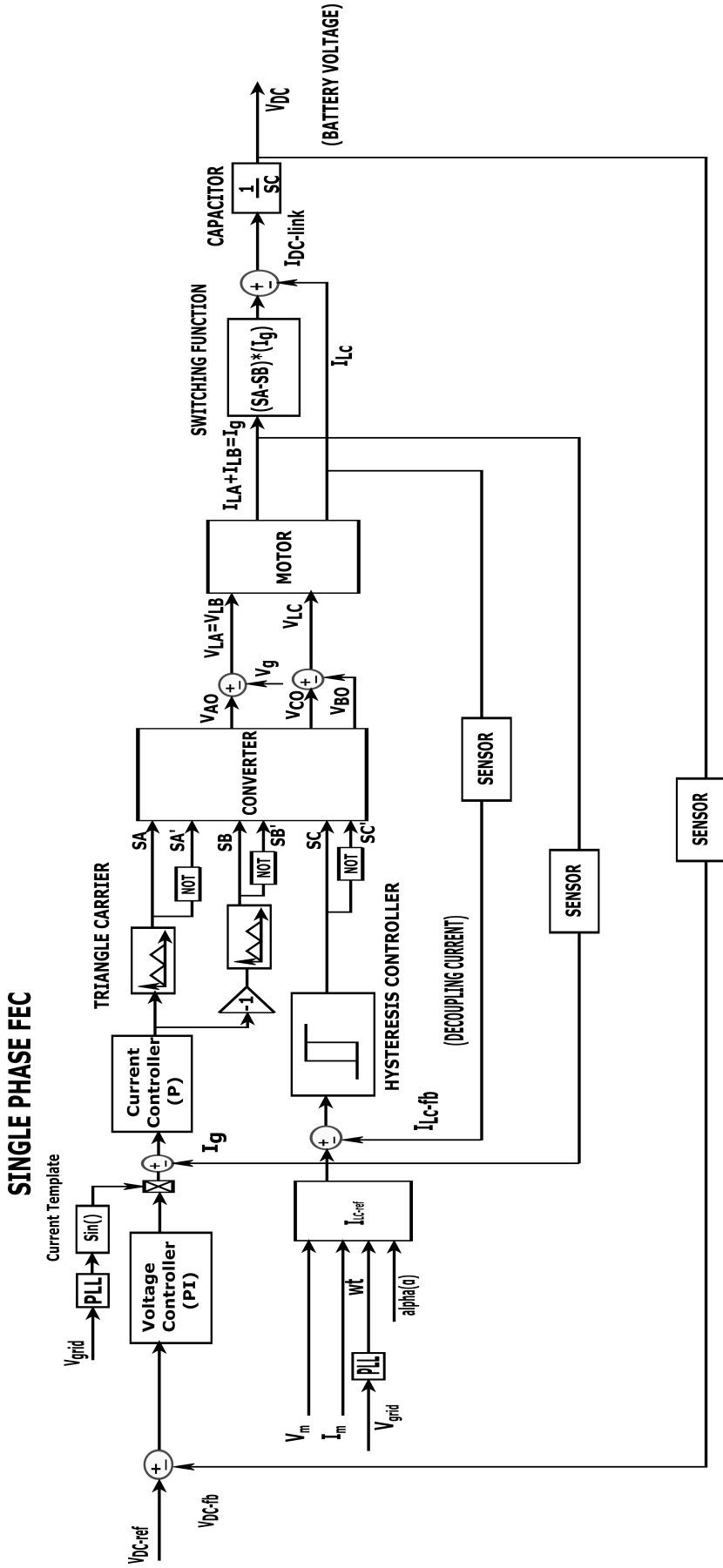


Figure 3.7: Control scheme for IBC topology using Hysteresis controller.

Chapter 4

Motor Model and Simulation Results

4.1 Performance of the IBC

There must be no torque produced in the induction motor during the charging in any electric vehicle integrated charging scheme. The induction motor winding currents are I_{sA} , I_{sB} , and I_{sC} . In the IBC scheme, these currents can be defined as in Eq.(4.1). The mathematical equations analysis of the induction motor is carried out in terms of winding currents.

$$\begin{aligned}I_{sA} &= I_{in}(t) = I_g \cos(\omega t) \\I_{sB} &= I_{in}(t) = I_g \cos(\omega t) \\I_{sC} &= I_{decoupling}(t) = I_{L_C} \cos(\omega t - \frac{\pi}{4})\end{aligned}\tag{4.1}$$

Change of reference frame is a helpful technique in analyzing electric machines. In our further analysis, Clarke's transformation is used in which three-phase quantities (ABC) are converted to an orthogonal stationary reference frame called the γ -frame [1]. The transformation equation involved is mentioned in Eq.(4.2).

$$\begin{bmatrix} I_{s\alpha} \\ I_{s\beta} \\ I_{s\gamma} \end{bmatrix} = \frac{2}{3} \begin{bmatrix} 1 & \frac{-1}{2} & \frac{-1}{2} \\ 0 & \frac{\sqrt{3}}{2} & \frac{-\sqrt{3}}{2} \\ \frac{1}{2} & \frac{1}{2} & \frac{1}{2} \end{bmatrix} \begin{bmatrix} I_{sA} \\ I_{sB} \\ I_{sC} \end{bmatrix} \quad (4.2)$$

Here, $I_{s\gamma}$ represents the common mode current in the windings. In our case $I_{sA} = I_{sB}$ and substituting Eq.(4.1) in Eq.(4.2), the following can be obtained.

$$I_{s\alpha} = \frac{I_{sB} - I_{sC}}{3} \quad (4.3)$$

$$I_{s\beta} = \frac{I_{sB} - I_{sC}}{\sqrt{3}} \quad (4.4)$$

$$I_{s\gamma} = \frac{I_{sA} + I_{sB} + I_{sC}}{3} \quad (4.5)$$

From, Eq.(4.3) and Eq.(4.4) it can be noted that

$$\sqrt{3}I_{s\alpha} = I_{s\beta} \quad (4.6)$$

Here, $I_{s\gamma}$ represents the common-mode current in the windings. In this case, $I_{sA} = I_{sB}$, since the windings A and B are connected in a parallel and symmetrical manner. In the analysis, the motor parameters used are Stator Resistance (R_s), Rotor Resistance (R_r), Stator Leakage Inductance (L_s), Rotor Leakage Inductance (L_r) and Mutual Inductance (L_m). Additionally, the relations $L_{ss} = L_m + L_s$ and $L_{rr} = L_m + L_r$ hold true.

The stator voltage equations describing the induction motor (IM) dynamics in the stationary $\alpha\beta$ -frame are given as in Eq.(4.7) and Eq.(4.8).

$$V_{s\alpha} = R_s I_{s\alpha} + L_{ss} \frac{dI_{s\alpha}}{dt} + L_m \frac{dI_{r\alpha}}{dt} \quad (4.7)$$

$$V_{s\beta} = R_s I_{s\beta} + L_{ss} \frac{dI_{s\beta}}{dt} + L_m \frac{dI_{r\beta}}{dt} \quad (4.8)$$

The rotor voltage equations describing the induction motor dynamics in the stationary $\alpha\beta$ -frame are given as in Eq.(4.9) and Eq.(4.10).

$$R_r I_{r\alpha} + L_{rr} \frac{dI_{r\alpha}}{dt} + L_m \frac{dI_{s\alpha}}{dt} + \omega_r L_m I_{s\beta} + \omega_r L_{rr} I_{r\beta} = 0 \quad (4.9)$$

$$R_r I_{r\beta} + L_{rr} \frac{dI_{r\beta}}{dt} + L_m \frac{dI_{s\beta}}{dt} - \omega_r L_m I_{s\alpha} - \omega_r L_{rr} I_{r\alpha} = 0 \quad (4.10)$$

When the electric vehicle is in charging mode, it will be in a still position and will not move. This emulates the case when $\omega_r = 0$. This condition along with substitution of Eq.(4.6) in Eq.(4.9), Eq.(4.10) gives,

$$R_r I_{r\alpha} + L_{rr} \frac{dI_{r\alpha}}{dt} + L_m \frac{dI_{s\alpha}}{dt} = 0 \quad (4.11)$$

$$R_r I_{r\beta} + L_{rr} \frac{dI_{r\beta}}{dt} + \sqrt{3} L_m \frac{dI_{s\alpha}}{dt} = 0 \quad (4.12)$$

Multiplying by $\sqrt{3}$ on both sides of Eq.(4.11),

$$R_r (\sqrt{3} I_{r\alpha}) + L_{rr} \frac{d(\sqrt{3} I_{r\alpha})}{dt} + \sqrt{3} L_m \frac{dI_{s\alpha}}{dt} = 0 \quad (4.13)$$

Comparing Eq.(4.12) and Eq.(4.13),

$$\sqrt{3} I_{r\alpha} = I_{r\beta} \quad (4.14)$$

The electromagnetic torque (T_{em}) generated by an induction motor is given by the expression

$$T_{em} = \frac{3}{2} \frac{P}{2} L_m [I_{r\alpha} I_{s\beta} - I_{r\beta} I_{s\alpha}] \quad (4.15)$$

Substituting Eq.(4.14) in Eq.(4.15),

$$T_{em} = \frac{3\sqrt{3}}{2} \frac{P}{2} L_m [I_{r\alpha} I_{s\alpha} - I_{r\alpha} I_{s\alpha}] = 0 \quad (4.16)$$

From Eq.(4.16), it can be concluded that the integrated battery charger circuit will not produce any torque in the motor winding during the charging phase of EV.

4.1.1 Power Rating of IBC

In single-phase IBC with FEC configuration and with active power decoupling, two motor windings are connected in parallel and used as interfacing inductors on the grid side. Third winding is used as an energy storage inductor in ripple power decoupling circuit to reduce the DC link voltage ripple. As power transfer, i.e., from AC (grid side) to DC (battery), is happening through the motor windings, the power rating of the IBC is decided by the power rating of the motor, i.e., current through the motor windings. Let the rated current per phase of the machine be I_{ph} . In the FEC configuration, two motor windings are connected in parallel and supply the maximum of $2I_{ph}$ current to the batteries.

The power rating of this IBC and motor are,

$$P_{IBC} = 2V_g I_g, P_m = 3V_{ph} I_{ph} \quad (4.17)$$

Hence the ratio of power rating of IBC to that of the motor is,

$$\frac{P_{IBC}}{P_m} = \frac{2V_g}{3V_{ph}} \quad (4.18)$$

Hence with the IBC, the power rating of the charger can be increased more than the power rating of the onboard charger of the vehicle.

4.2 Simulation Results

4.2.1 Simulation Parameters

The proposed IBC is simulated in a MATLAB-Simulink environment. The values of various parameters for simulation are given in Table 4.1

Table 4.1: Simulation Parameters for IBC

Parameters	Variable	Value
Grid Voltage	V_g	230V(rms)
DC link Voltage	V_{DC}	400V
DC link Capacitance	C	800uF
Switching frequency	f_s	10KHz
Max.Power	P_{out}	2kW
Motor stator leakage inductance	L_s	10mH
Motor rotor leakage inductance	L_r	10mH
Motor mutual inductance	L_m	82mH
Stator resistance	R_s	1Ω
Rotor resistance	R_r	1.1Ω

4.2.2 Steady State Behaviour of FEC

Initially, the FEC is simulated without active decoupling of power. In (Fig.4.1) steady-state waveforms are shown. DC-bus has a significant ripple in it (5% of nominal value). Also, the decoupling current is at zero level.

When the decoupling loop is engaged in the system, a set reference I_{dec} current flows through the C-phase winding of IM. (Fig.4.2) shows the response of FEC for the same. It can be observed from (Fig.4.2) that ripple in DC-bus voltage is reduced significantly (from 5% to 1%) of nominal DC-bus voltage. The current flowing in the C phase winding is I_{dec}

should be 45° lagging with grid current I_g . (Fig.4.3) shows the current waveforms of the FEC.

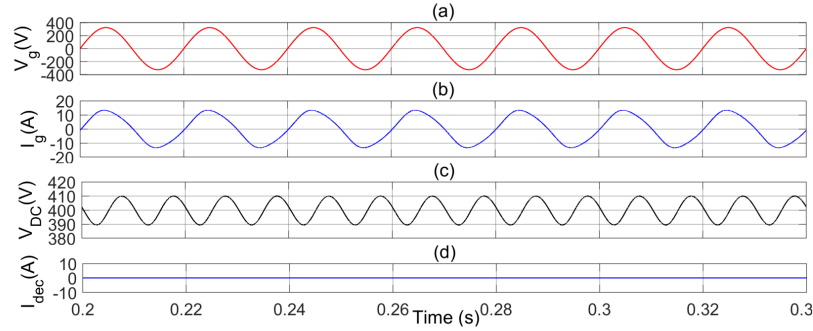


Figure 4.1: Steady state waveforms for 1- ϕ FEC without decoupling : (a) Grid Voltage V_g (V), (b) Grid Current I_g (A), (c) DC-link Voltage V_{DC} (V),(d) Decoupling Current I_{dec} (A)

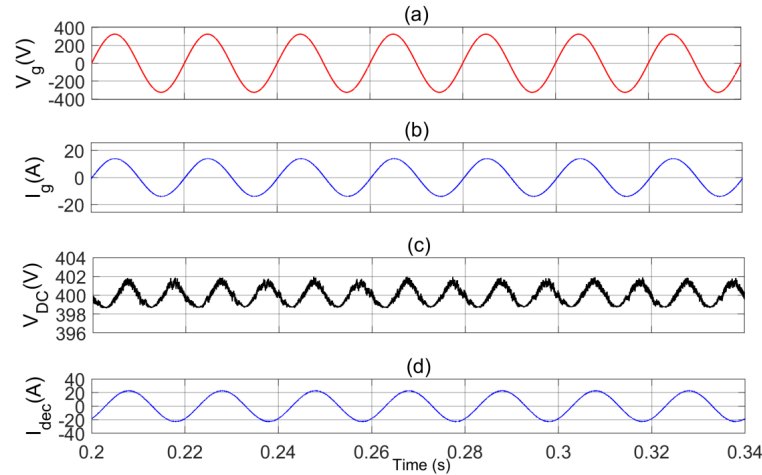


Figure 4.2: Steady state waveforms for 1- ϕ FEC with decoupling : (a) Grid Voltage V_g (V), (b) Grid Current I_g (A), (c) DC-link Voltage V_{DC} (V), (d) Decoupling Current I_{dec} (A)

4.2.3 Transient Behaviour of FEC

In our study, the transient behaviour of the FEC is studied using :

- Increase the load from half load to rated load suddenly at time $t = 0.5$ sec
(Step Response) .

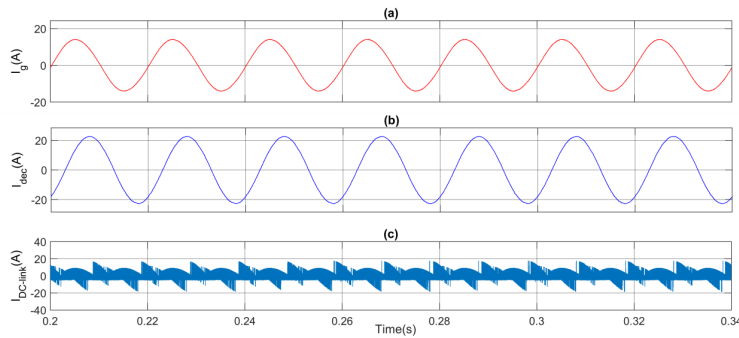


Figure 4.3: Steady state current waveforms for 1- ϕ FEC with decoupling : (a) Grid Current I_g (A), (b) Decoupling Current I_{dec} (A), (c) DC-link Current I_{DC_link} (A).

- Uniformly increase the reference DC bus voltage from 380 V to 420 V, starting from time $t = 0.5$ sec (Ramp Up Response).
- Uniformly decrease the reference DC bus voltage from 380 V to 420 V, starting from time $t = 0.5$ sec (Ramp Down Response).

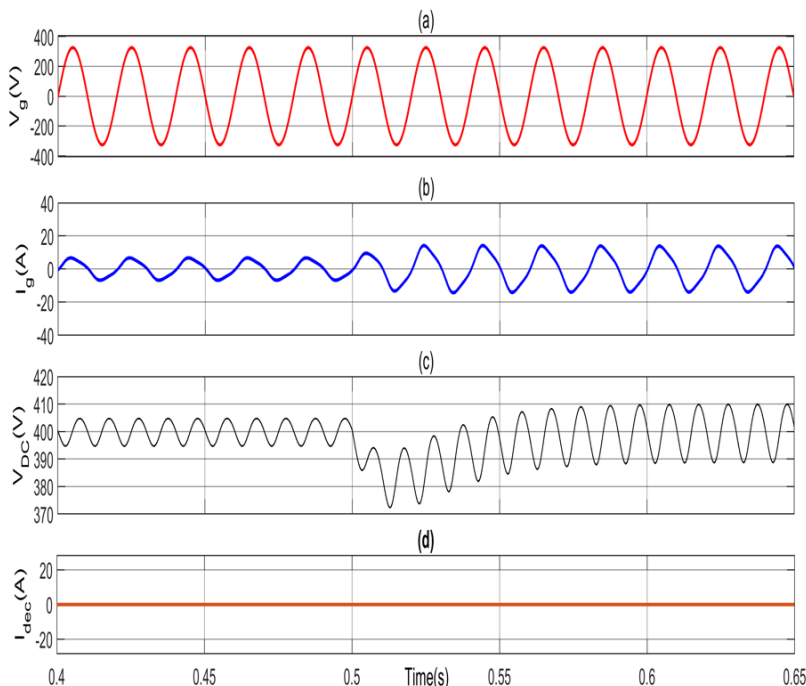


Figure 4.4: Transient waveforms for step load change from half load to full load at time $t = 0.5$ s without decoupling.

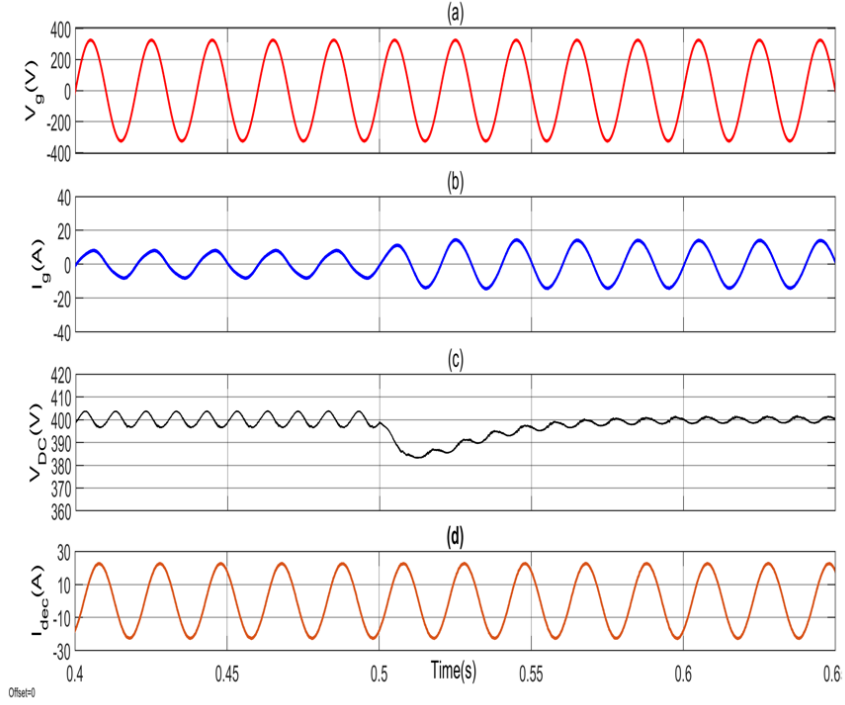


Figure 4.5: Transient waveforms for step load change from half load to full load at time $t = 0.5$ s with decoupling.

(Fig.4.4) shows the FEC behavior for load variation without decoupling phenomenon. It is evident from the (Fig.4.4) above that DC bus voltage responds well and attain its desired value (within 5-6 fundamental cycles), but there is a high voltage ripple. In (Fig.4.5), FEC response for load variation along with decoupling phenomenon is shown. In this case, the ripple in DC bus voltage is at its minimal level (1% of nominal DC bus voltage). Also, DC bus voltage attains its desired value within 5-6 fundamental cycles. These responses are like step responses of the system.

(Fig.4.6) shows the response of FEC for a uniform increase in reference DC bus voltage from 380 V to 420 V for three fundamental cycles. It can be observed that the actual DC link voltage tracks the set reference. In (Fig.4.7) FEC response for an uniform decrease in reference DC bus voltage (from 420 V to 380 V) is shown.

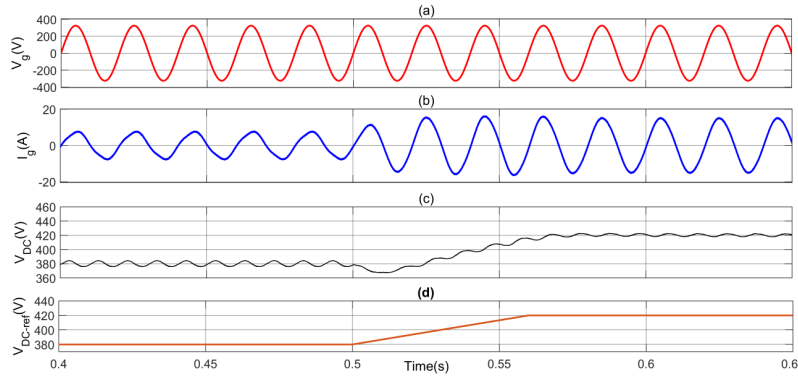


Figure 4.6: Transient waveforms for a uniform increase in reference DC bus voltage (from 380 V to 420 V) for three cycles with decoupling (Ramp-Up Response).

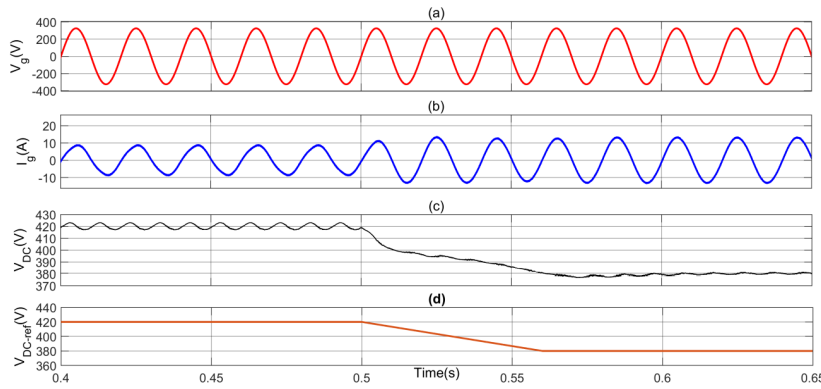


Figure 4.7: Transient waveforms for a uniform increase in reference DC bus voltage (from 380 V to 420 V) for three cycles with decoupling (Ramp-Down Response).

4.2.4 Simulation Results of IBC topology with Hysteresis Controller

The simulation results in (Fig.4.8) show the behavior of IBC for a step load change at time $t = 0.5$ s. It can be observed that output DC bus voltage is at set reference value with 1% ripple at steady state. For load variation, the grid current I_g and DC bus voltage V_{DC} respond quite well and attain their steady-state values.

(Fig.4.9a) shows the response of IBC topology for a uniform increase in reference DC bus voltage is changed from 380 V to 420 V for three fundamental cycles. It can be observed that the actual output DC bus voltage tracks the set reference voltage. In (Fig.4.9b)

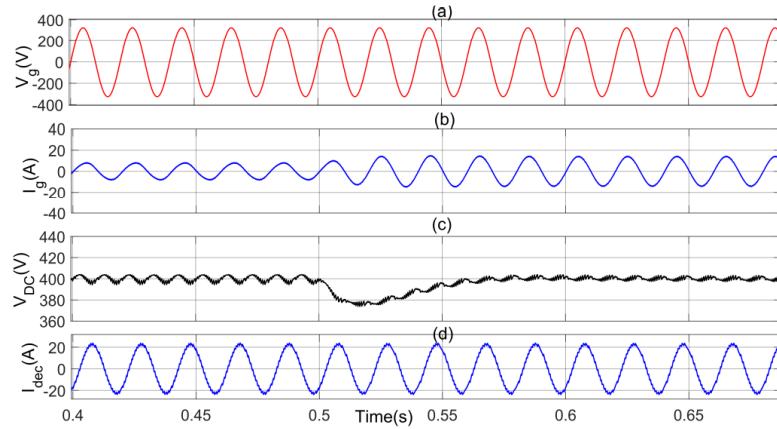
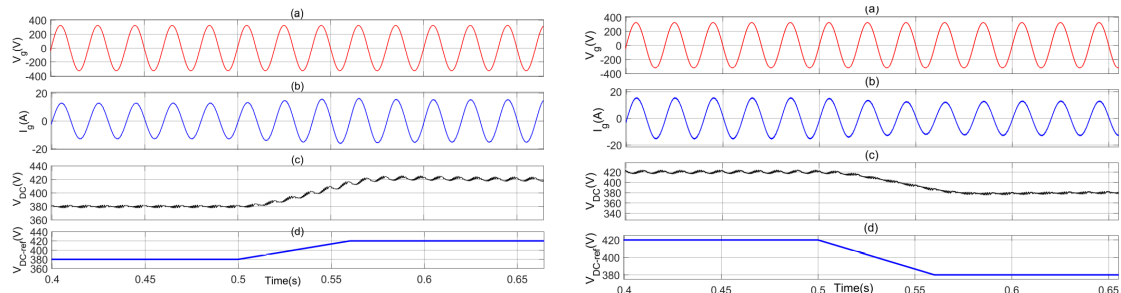


Figure 4.8: Simulation results with hysteresis control based decoupling engaged (step change in load from half load to full load at $t = 0.5\text{ s}$).



(a) Simulation results for an increase in V_{DC-ref} . (b) Simulation results for a decrease in V_{DC-ref} .

Figure 4.9: (a) Ramp-Up and (b) Ramp-Down Responses of the Hysteresis Control Based Decoupling Loop engaged in IBC Circuit

response of IBC topology for a uniform decrease in reference DC bus voltage is observed. At time $t = 0.5$ sec, the DC-bus reference is changed from 420 V to 380 V for three fundamental cycles. Actual output DC bus voltage tracks the set reference. This analysis confirms that IBC topology responds quite satisfactorily to the load, DC bus reference change.

Chapter 5

Conclusions and Future Works

Fossil fuels powered internal combustion engine (ICE) vehicles increase global warming and significantly impact the atmosphere. This global concern increases the demand for electric vehicles (EV), which can quickly compete and replace the existing ICE automobiles. The significant challenges for its wide acceptance are initial cost, range anxiety, and availability of charging infrastructure. There is a continuous evolution of new technologies and innovative designs in the EV industry.

This report discusses a hysteresis controller-based active power decoupling scheme for Integrated Battery Charger (IBC). IBC implies that the power-train components of the EV itself can be utilized to charge the battery. This scheme has inherent short circuit fault protection and easier control implementation than a conventional P controller. This control scheme efficiently controls decoupling current and is viable for higher power levels, fast charging of EVs. This results in improved battery life and better performance. Simulation results are presented for the proposed control scheme, and load variation from half to rated load is simulated. The variation in output DC bus voltage reference(a uniform increase from 380V to 420V and uniform decrease from 420V to 380V is also simulated). Due to the advantages of inherent short circuit fault protection, easier controller implementation, precise control of current in the system, the proposed hysteresis control is a viable control scheme for IBC. Simulation and experimental results of both steady-state and transients

were provided. Also, the results with and without decoupling circuits are discussed and compared.

Following is a brief list of tasks that can be completed in the future :

- **Hardware Implementation of the IBC Charger Circuit :**

Currently, the IBC circuit has been validated from simulation results. The results are also to be validated by implementing the circuit on hardware. This would also require the proper selection of capacitors, inductors, gate driver ICs, inverter modules, IGBT switches, and digital signal processors to implement the control algorithm for active power decoupling.

- **Implementation of Other Control Schemes :**

Currently, the control loop uses standard P, PI controllers for maintaining UPF and ensuring output DC voltage. Sine-triangle PWM is used for the generation of gating pulses. The decoupling loop engaged uses a hysteresis controller. These controllers can reduce the output voltage ripple from 5% to 0.8%. However, there are other control schemes, which may further improve the performance of the system. Some of the other control schemes to be explored are Two-Degree Freedom Controller, Proportional Resonant Controller, and Advanced Fixed Frequency Hysteresis Controller.

Bibliography

- [1] M. Kompella, P. Yadav, and R. S. Kaarthik, “A single phase integrated battery charger with active power decoupling for electric vehicles,” in *2020 IEEE International Conference on Power Electronics, Drives and Energy Systems (PEDES)*, 2020, pp. 1–6.
- [2] K. Morrow, D. Karner, and J. E. Francfort, “Plug-in hybrid electric vehicle charging infrastructure review,” 2008.
- [3] G. Pellegrino, E. Armando, and P. Guglielmi, “An integral battery charger with power factor correction for electric scooter,” *IEEE Transactions on Power Electronics*, vol. 25, no. 3, pp. 751–759, 2010.
- [4] M. Yilmaz and P. T. Krein, “Review of battery charger topologies, charging power levels, and infrastructure for plug-in electric and hybrid vehicles,” *IEEE transactions on Power Electronics*, vol. 28, no. 5, pp. 2151–2169, 2012.
- [5] F. Musavi, M. Edington, W. Eberle, and W. G. Dunford, “Energy efficiency in plug-in hybrid electric vehicle chargers: Evaluation and comparison of front end ac-dc topologies,” in *2011 IEEE Energy Conversion Congress and Exposition*. IEEE, 2011, pp. 273–280.
- [6] B. Bilgin, E. Dal Santo, and M. Krishnamurthy, “Universal input battery charger circuit for phev applications with simplified controller,” in *2011 Twenty-Sixth Annual*

IEEE Applied Power Electronics Conference and Exposition (APEC). IEEE, 2011, pp. 815–820.

- [7] H. R. Vangala, “Single phase integrated battery charger for electric vehicles,” IIST Master’s Thesis 2021.
- [8] B. Singh, B. N. Singh, A. Chandra, K. Al-Haddad, A. Pandey, and D. P. Kothari, “A review of single-phase improved power quality ac-dc converters,” *IEEE Transactions on industrial electronics*, vol. 50, no. 5, pp. 962–981, 2003.
- [9] D. Xu, J. Zhang, W. Chen, J. Lin, and F. C. Lee, “Evaluation of output filter capacitor current ripples in single phase pfc converters,” in *Proceedings of the Power Conversion Conference-Osaka 2002 (Cat. No. 02TH8579)*, vol. 3. IEEE, 2002, pp. 1226–1231.
- [10] Y. Sun, Y. Liu, M. Su, W. Xiong, and J. Yang, “Review of active power decoupling topologies in single-phase systems,” *IEEE Transactions on Power Electronics*, vol. 31, no. 7, pp. 4778–4794, 2016.
- [11] M. Su, P. Pan, X. Long, Y. Sun, and J. Yang, “An active power-decoupling method for single-phase ac–dc converters,” *IEEE Transactions on Industrial Informatics*, vol. 10, no. 1, pp. 461–468, 2014.
- [12] S. Tripathi and R. Batra, “Operation and control of single phase front end converter,” in *2020 First IEEE International Conference on Measurement, Instrumentation, Control and Automation (ICMICA)*, 2020, pp. 1–6.
- [13] P. Yadav, V. Vidya, and R. S. Kaarthik, “A voltage sensor-less single-phase unity power factor ac-dc front-end converter,” in *2019 IEEE Transportation Electrification Conference (ITEC-India)*, 2019, pp. 1–6.

- [14] A. Kusko, *Power quality in electrical systems*. McGraw-Hill Education, 2007.
- [15] S. Bala, T. Tengnér, P. Rosenfeld, and F. Delince, “The effect of low frequency current ripple on the performance of a lithium iron phosphate (lfp) battery energy storage system,” in *2012 IEEE Energy Conversion Congress and Exposition (ECCE)*. IEEE, 2012, pp. 3485–3492.
- [16] T.-H. Kim, J.-B. Jeong, B.-H. Lee, D.-H. Shin, H.-S. Song, B.-H. Kim, and H.-J. Kim, “Analytical study on low-frequency ripple effect of battery charging,” in *2012 IEEE Vehicle Power and Propulsion Conference*. IEEE, 2012, pp. 809–811.